Article

Determination of Aerodynamic Drag Coefficients of Longitudinal Finned Tubes of LNG Ambient Air Vaporizers Using CFD and Experimental Methods

Filip Lisowski [1,*] and Edward Lisowski [2]

1 Department of Machine Design and Composite Structures, Cracow University of Technology, ul. Warszawska 24, 31-155 Cracow, Poland
2 Department of Applied Informatics, Cracow University of Technology, ul. Warszawska 24, 31-155 Cracow, Poland
* Correspondence: filip.lisowski@pk.edu.pl

Abstract: This paper presents the results of numerical and experimental studies of wind action on longitudinal finned tubes of LNG ambient air vaporizers. The main objective of the study was to determine the aerodynamic drag coefficients for longitudinal finned tubes with different number of fins considering various directions of wind action. Numerical calculations were performed using CFD analysis, while experimental tests were carried out in a wind tunnel test stand. The obtained results indicate the variation of tube loads depending on the number of fins and the direction of wind action and can be used in the design of ambient air vaporizers.

Keywords: longitudinal finned tubes; LNG ambient air vaporizers; aerodynamic drag coefficients; CFD analysis; wind tunnel tests

1. Introduction

Liquefied natural gas (LNG) is increasingly used both as a source of energy and in production processes. Due to the possibility of its delivery by sea and by land, local regasification stations are built in various remote locations, often in open spaces or near coastal areas where strong winds occur. The basic devices of the LNG regasification stations are cryogenic storage tanks [1,2] and ambient air vaporizers (AAVs) shown in Figure 1. Aluminum profiles in the form of longitudinal finned tubes are most commonly used in the construction of ambient air vaporizers. Aluminum alloys are used because of their good properties in terms of both thermal conductivity and the possibility to extrude finned profiles with complex geometry. There are two typical AVV design variants: with a natural draft and with a forced draft. In the first variant, the aluminum profiles are not covered and the air inflow is possible from all sides. For the second variant, the profiles are shielded and the airflow is forced inside the housing by additional fans mounted on top of the vaporizer [3]. The larger the external surface area of longitudinally finned tubes, the more heat is collected by the fins and thus more energy is provided for the vaporization process [4]. Design and optimization problems related to the ambient air vaporizers with longitudinal finned tubes have been of interest to the authors of several previous publications. One of the problems addressed was the determination of convective heat transfer coefficients for longitudinal finned tubes and optimization for heat transfer efficiency. Jeong et al. (2006) [5] presented the results of a Computational Fluid Dynamics (CFD) analysis of natural convection heat transfer for the longitudinally finned tube. The obtained heat transfer coefficients were used to determine the Nusselt number outside the tube. Niezgoda-Żelasko and Żelasko (2014) [6] presented the results of the experimental studies of the heat transfer on the outer surface of longitudinal finned tubes with a wavy shape of fins. The authors delivered the dimensionless relationships to determine the

values of the heat transfer coefficients at the outer surface of the longitudinal finned tube for free and mixed convection conditions. In turn, Kopeć and Niezgoda-Żelasko (2021) [7] presented the optimization results of the geometric parameters of longitudinal finned tubes under mixed convection conditions. The tubes with fins of wavy shapes were intended to use in a heat pump evaporator. Sun et al. (2018) [8] studied the heat transfer between ambient air and LNG under supercritical conditions. The CFD modeling was proposed to investigate the supercritical flow of liquefied natural gas inside the ambient air vaporizer. In addition, the results of longitudinal finned tube geometry optimization were delivered. Wang et al. (2022) [9] proposed a calculation model of coupled heat and mass transfer from ambient air to LNG inside the tube. The model was intended to analyze the heat transfer process in ambient air vaporizers including LNG phase change inside longitudinal finned tubes.
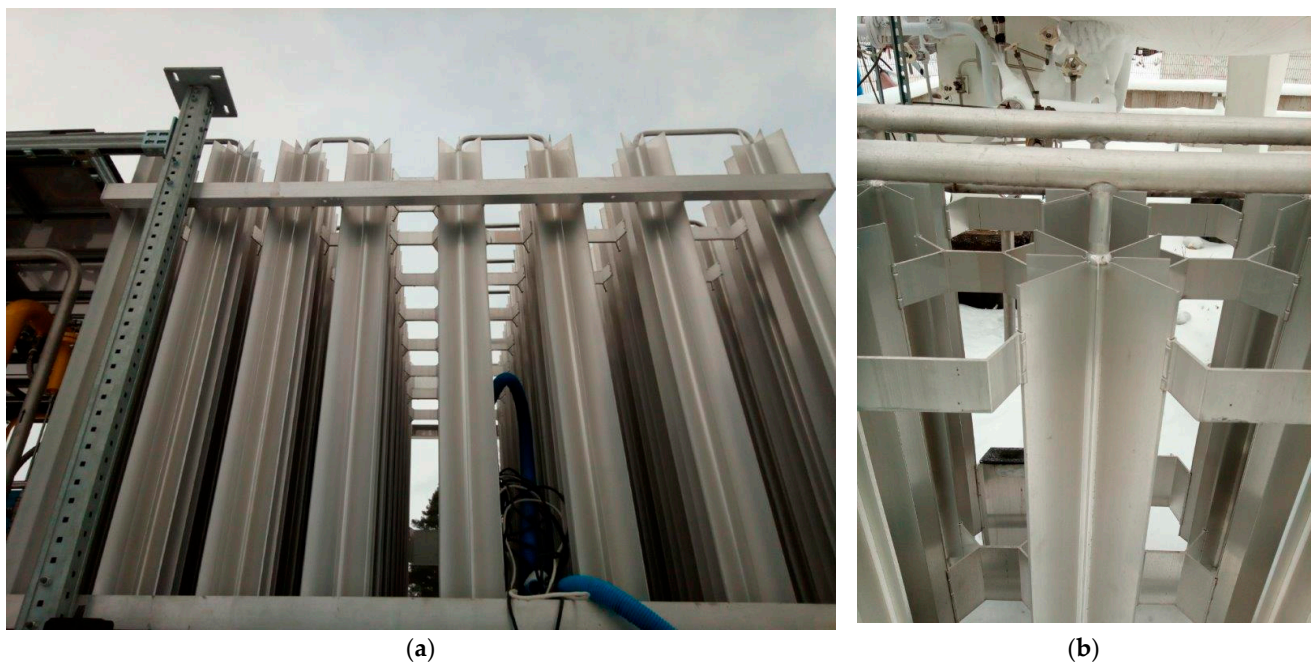

(a)   (b)

Figure 1. Ambient air vaporizer (**a**) general view; (**b**) detailed view on the aluminum finned tube.

Another issue raised in publications was the problem of longitudinal finned tubes frosting during ambient air vaporizer operation. Jeong et al. (2009) [10] presented a study on the optimum design of AAV longitudinal finned tube geometry by applying numerical and experimental analyses. As a result, the recommended relations of the fins' dimensions were proposed for optimal heat transfer both with and without frosting. Chen et al. (2013) [11] presented a study on the thermal conductivity of frost accumulated on the finned tube of cryogenic vaporizers using a fractal method. In turn, studies presented by Kuang et al. (2015) [12], Liu et al. (2016) [13], Liu et al. (2017) [14], Lee et al. (2018) [15], and Liu et al. (2021) [16] were concerned with the analysis of ambient air vaporizer operation, including frosting conditions and their influence on heat transfer efficiency.

Ambient air vaporizers can be large, even reaching several meters in height, due to the need to obtain a sufficiently high efficiency. The large size causes AVVs to be subjected to significant wind exposure. A study on the wind action on ambient air vaporizer structures was presented by Lisowski and Lisowski (2022) [17]. CFD analysis was applied to investigate the influence of a longitudinally finned tube arrangement on the wind load. In addition, the effect of various spacing pitches of the tubes and different wind directions were analyzed. It was noticed that, depending on the above parameters, individual tubes can be significantly overloaded compared to other tubes in the AVV structure.

There are several methods to evaluate and compare the effect of wind action on ambient air vaporizer structures. The essential quantity to be determined for the further

estimation of finned tube strength, as well as that of the entire AAV structure, is the wind force. In general, calculation procedures in accordance with the relevant wind standards can be used or CFD analysis can be applied. With regard to the whole AAV structure, including the longitudinal finned tube array, underframe, and support as well as accounting for factors arising from the surrounding terrain and wind fluctuations, the calculations can be carried out in accordance with Eurocode 1991-1-4 [18], which refers to wind action on structures. However, in the case of unshielded vaporizers, such calculations are partially simplified because they refer to the flat reference area of the entire structure (orthogonal projection of the surface) that resists the wind action. Therefore, the effect of wind action on individual finned tubes, which are profiles with sharp edges and complex shapes, is not considered. On the other hand, considering the wind action on a single finned tube profile according to the Eurocode procedure, it is possible to determine the wind load on a structural element with sharp section edges. However, the above calculation procedure requires the assumption of aerodynamic drag coefficients depending on the profile cross section. The wind force according to Eurocode is given by Equation (1), whereas the peak velocity pressure is given by Equation (2). From Equations (1) and (2) it follows that the aerodynamic drag coefficient can be determined using the formula given by Equation (3).

$$F_w = c_f c_d \cdot c_f \cdot q_p(z_e) \cdot A_{ref} \tag{1}$$

$$q_p(z_e) = 0.5 \cdot \rho \cdot v^2(z_e) \tag{2}$$

$$c_f = \frac{F_w}{0.5 \cdot \rho \cdot v^2(z_e) \cdot A_{ref}} \tag{3}$$

where: F_w—wind force [N], $c_f c_d$—structural factor ($c_f c_d = 1$, for structures lower than 15 m), c_f—force coefficient for the structure or structural element (drag coefficient), $q_p(z_e)$—peak velocity pressure [Pa] at reference height z_e [m], A_{ref}—reference area for the structure or structural element [m^2], ρ—air density [kg/m^3], $v(z_e)$—wind speed at reference height [m/s^2].

For the above formulas, once the value of the drag coefficient and the cross-sectional area in the plane perpendicular to the wind direction are known, the value of the aerodynamic force acting on the object can be estimated. In general, this method is used while designing many industrial facilities, for its part, aerodynamic coefficients are usually determined experimentally in wind tunnels. Some of these studies were reported in publications. For example, Matys et al. (2011) [19] determined the aerodynamic coefficient for various blade types of a carousel wind turbine based on wind tunnel experiments, whereas Wu et al. (2019) [20] developed an aerodynamic measurement on horizontal axis wind turbines in order to estimate the loads of blades in atmospheric conditions. Wind tunnel tests were performed to validate the aerodynamic measurement platform. Zaghi et al. (2016) [21] presented the results of numerical simulations of the flow around a three-bladed wind turbine with a horizontal axis. The aim of the research was to analyze the boundary conditions to be used in numerical simulations, accounting for blockage effects in wind tunnel experiments for large wind turbines. In turn, Augustyn (2014) [22] determined drag coefficients and loads on a mobile elevating working platform. Various angles of wind attack are considered in wind tunnel tests. Damjanović et al. (2017) [23] presented the results of a CFD analysis of wind effects on eave frames. The obtained loads from the airflow analysis were then adopted for further static structural analysis. Flaga et al. (2016) [24] presented results of wind tunnel experiments for free-standing lighting protection masts placed on building roofs. The purpose of the study was to determine aerodynamic coefficients for further calculations of wind loads acting on the considered masts. Skeide et al. (2020) [25] studied the flow around circular ribbed cylinders, including the impact of ribs and surface roughness on the drag and vortex shedding.

For ambient air vaporizer design purposes, there is usually a need for a quick assessment and comparison of the wind impact on the vaporizer structure, considering the use of different finned tube profiles. In this paper, the results of the CFD analysis and wind

tunnel tests of wind effects on a single finned tube are presented. The aerodynamic drag coefficients were determined in order to calculate and compare the wind load acting on the longitudinally finned tubes. The effect of a different number of fins and various profile orientations with respect to the wind direction was studied.

2. Wind Tunnel Tests

In order to verify the results of the numerical studies, experimental tests were carried out using a small wind tunnel test stand, the scheme of which is shown in Figure 2 and the tunnel itself is shown in Figure 3. An axial fan with a maximum flow rate of 3110 m³/h and power of 200 W forced the airflow on the test stand. The fan diameter was 350 mm and the test section diameter was 250 mm. For the above parameters, a flow velocity of about 10 m/s was achieved. The force acting on the tested finned tube in the direction of airflow was measured using the one-component balance. A digital anemometer and a digital manometer were used to determine the air velocity and pressure in front of the tested finned tubes. The accuracy of the anemometer was ±2% and the manometer was ±0.3%.

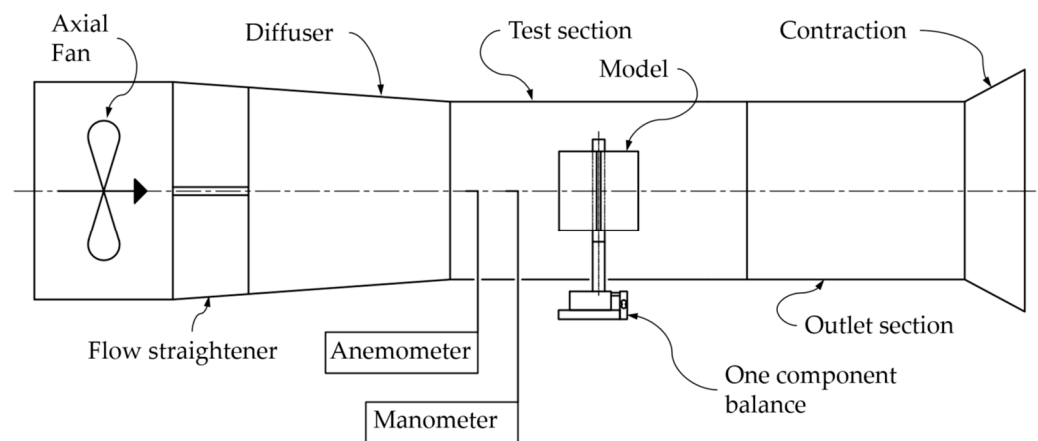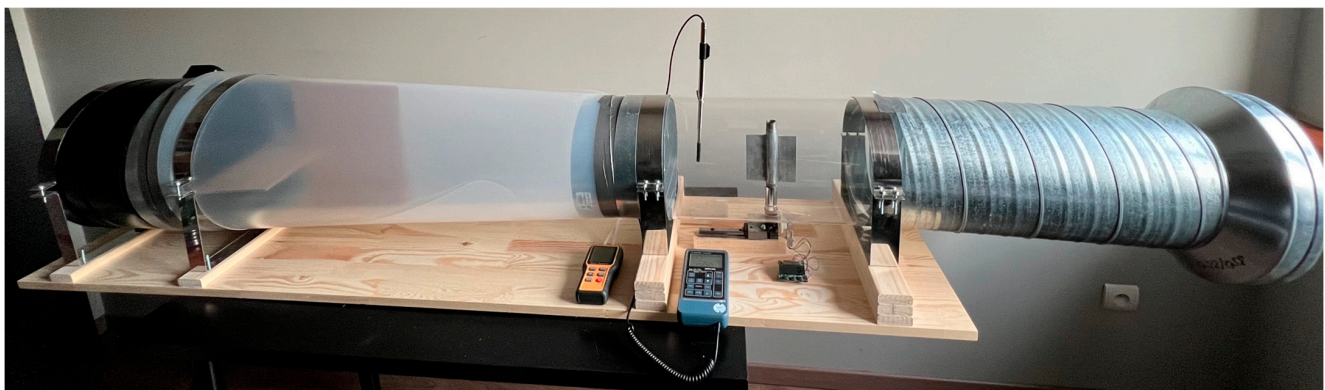**Figure 2.** Schematic diagram of the test stand.

Figure 3. Wind tunnel test stand.

3. Numerical Simulation

The analysis of wind action on the longitudinal finned tube profiles of LNG ambient air vaporizers was carried out using ANSYS/Fluent Release 2020 R2 software. First, discrete models were prepared for the considered profiles' geometries and mesh validation was conducted. Then, the flow type was determined to be turbulent and the boundary conditions were assigned. Finally, airflow simulations were carried out using the CFD software for three adopted profiles geometries and accounting for two wind directions, which are reflected in the profiles' orientations with respect to the airflow direction.

3.1. The Object of Study

Dedicated aluminum profiles in the form of tubes with longitudinally extruded fins are commonly used for the construction of LNG ambient air vaporizers. Typical designs are aluminum tubes with a number of fins from two to a dozen. The technologies of creating aluminum lamellas enable the production of fins with lengths several times greater than the central tube diameter. With central pipe diameters in the range of 25–30 mm, the height of the ribs can reach up to 200 mm, depending on the thickness. In this study, three cross sections of longitudinal finned tubes with the number of fins 2, 4, and 8 were accepted for analysis as shown in Figures 4 and 5. All profiles had the identical dimensions shown in Figure 5b and differed in the number of fins around the perimeter of the central tube. Profile sections of 100 mm in length were analyzed. Six cases were included in the analysis, as shown in Figure 6.
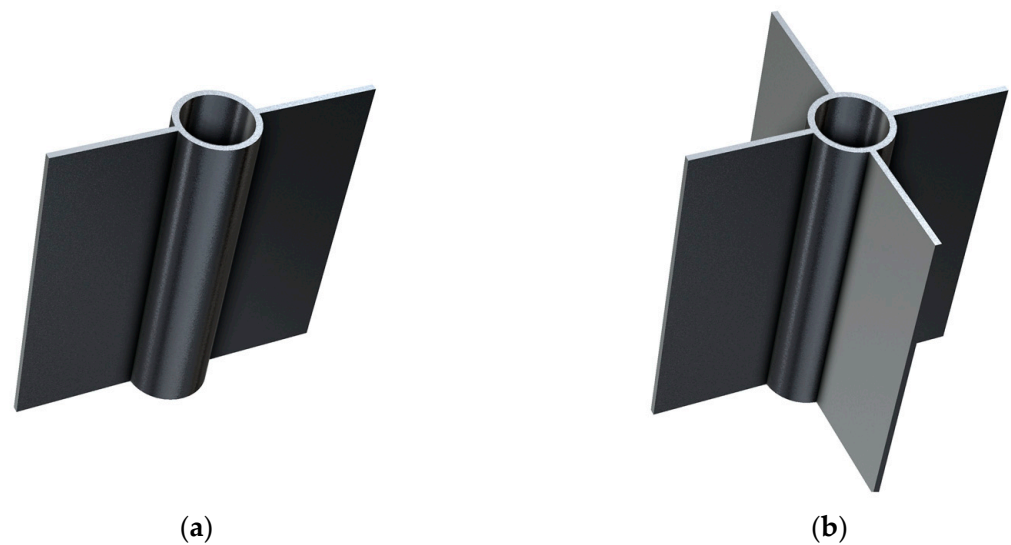

(**a**)   (**b**)
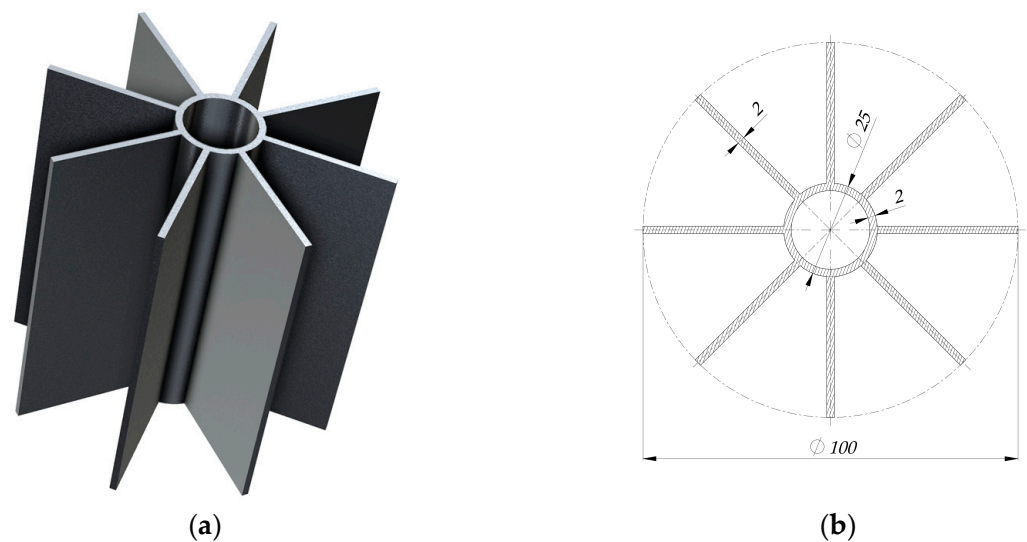
Figure 4. Geometry of longitudinal finned tubes with: (**a**) 2 fins; (**b**) 4 fins.

(**a**)   (**b**)

Figure 5. (**a**) Geometry and (**b**) cross-sectional dimensions of longitudinal finned tube with 8 fins.
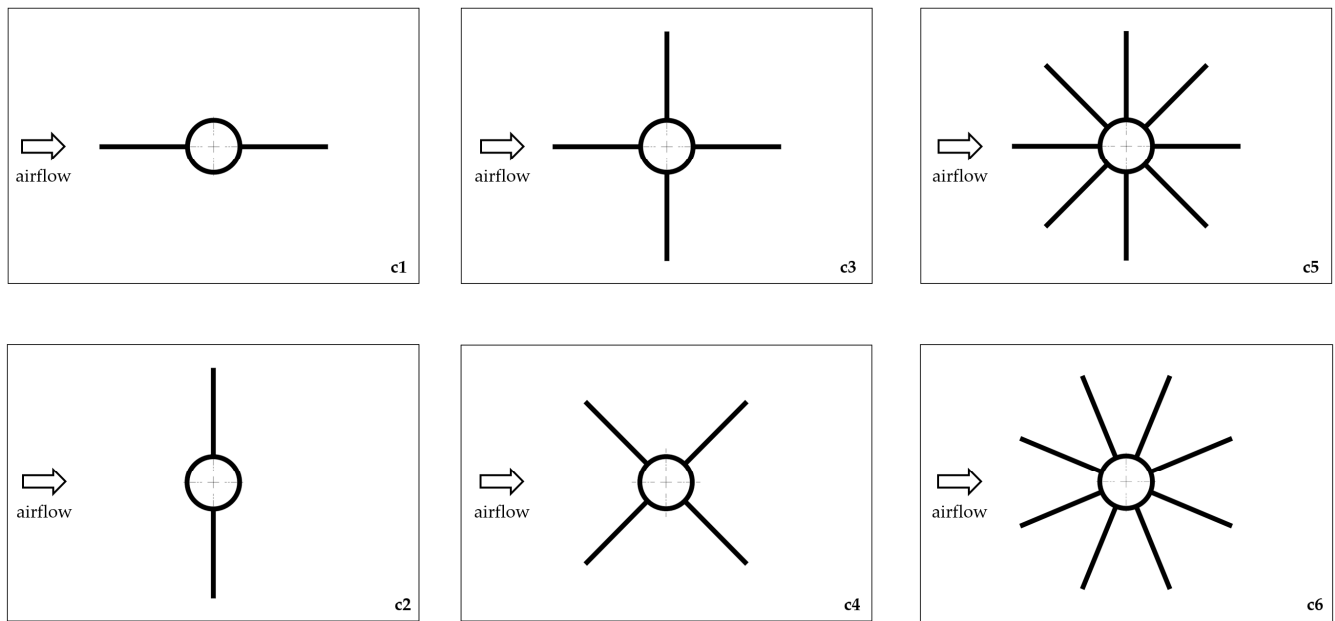
Figure 6. Analyzed cases (**c1**–**c6**) of profiles orientation.

3.2. Discrete Models and Mesh Validation

For each of the analyzed cases, a three-dimensional model of the computational domain was prepared considering the shape of the finned tube profile placed in a cylindrical volume with a diameter d = 250 mm and a length l = 1000 mm. An example of the meshed model with boundary conditions for the case c5 is shown in Figure 7, where v_{inlet} stands for wind velocity and p_{atm} is atmospheric pressure. The computational domains were discretized using irregular tetrahedrons elements.
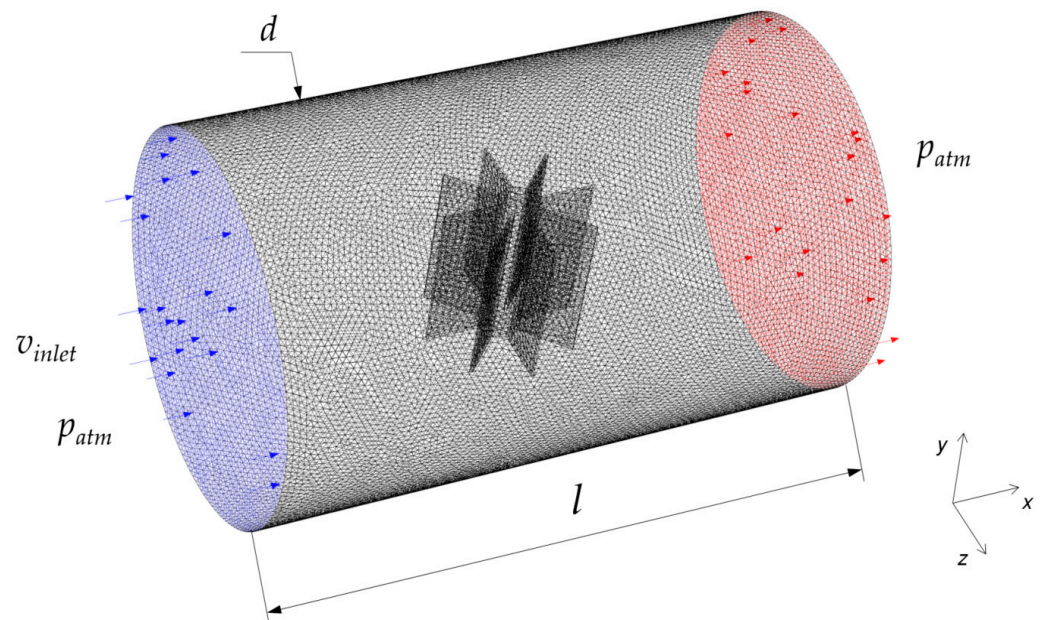

Figure 7. Discretized model with boundary conditions for the case c5.

The mesh quality adopted for further analysis was determined using a preliminary mesh independence test based on the case c5. For the mesh independence test, a wind velocity of 10 m/s was accepted. The results of the mesh validation analysis are shown in Figure 8, where points m1–m8 correspond to the results for different mesh qualities. It

can be seen that the results for the quality of the m6–m8 mesh are significantly similar to each other with the percentage error <0.5%. Therefore, the corresponding mesh quality was assumed for all other computational cases, resulting in approximately 100,000 finite elements.
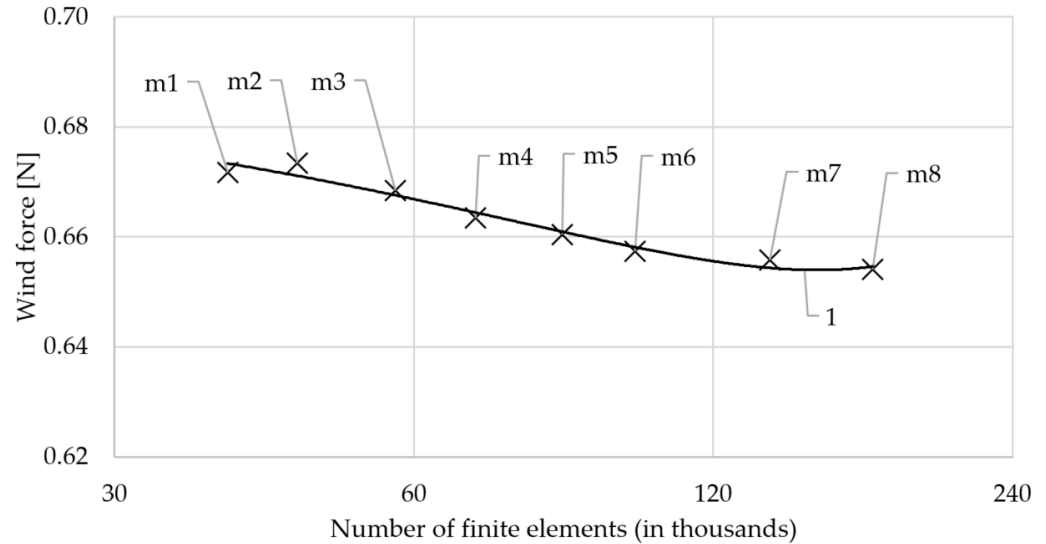

Figure 8. Mesh validation results based on case c5: (1) polynomial approximation of wind force for different mesh quality (m1–m8).

3.3. Governing Equations

The ANSYS Fluent solves the conservation equations of mass and momentum for all analyzed flows. The general form of the mass conservation equation is given by Equation (4), while the equation for the conservation of momentum is given by Equation (5). An additional energy conservation Equation (6) is solved for flows account for heat transfer or the compressibility of the fluid [26].

$$\frac{\partial \rho}{\partial t} + \nabla \cdot \rho \vec{v} = 0 \tag{4}$$

$$\frac{\partial}{\partial t}\left(\rho \vec{v}\right) + \vec{v} \cdot \nabla\left(\rho \vec{v}\right) = -\nabla p + \nabla \cdot \overline{\overline{\tau}} + \vec{F'}_b \tag{5}$$

$$\frac{\partial}{\partial t}\left(\rho e_t\right) + \nabla \cdot \left[\vec{v}\left(\rho e_t + p\right)\right] = \nabla \cdot \left[k\nabla T + \left(\overline{\overline{\tau}} \cdot \vec{v}\right)\right] + S_g \tag{6}$$

where: ρ is the fluid density, Nabla operator ∇ stands for the partial derivative with respect to all directions in the coordinate system, $\vec{v}$ is the velocity vector, p stands for static pressure, $\overline{\overline{\tau}}$ is the stress tensor, $\vec{F'}_b$ is for the body force per unit volume, e_t is total energy in the system, k is the thermal conductivity, T stands for temperature, and S_g include the heat of the chemical reaction and any defined volumetric heat sources.

3.4. Turbulence Model

For the purposes of CFD analysis, the type of flow had to be defined. There are no conditions for the occurrence of laminar flow for air flow around longitudinal finned tubes due to their complex geometry and high value of Reynolds number. Therefore, the standard k-ε turbulence model was adopted in the simulations. The kinetic energy of the turbulence and dissipation factor were computed on the basis of the transport Equations (7) and (8).

$$\frac{\partial(\rho k)}{\partial t} + \frac{\partial(\rho k u_i)}{\partial x_i} = \frac{\partial}{\partial x_j}\left[\left(\mu + \frac{\mu_t}{\sigma_k}\right)\frac{\partial k}{\partial x_j}\right] + G_k + G_b - \rho\varepsilon - Y_M + S_k \tag{7}$$

$$\frac{\partial(\rho\varepsilon)}{\partial t} + \frac{\partial(\rho\varepsilon u_i)}{\partial x_i} = \frac{\partial}{\partial x_j}\left[\left(\mu + \frac{\mu_t}{\sigma_k}\right)\frac{\partial\varepsilon}{\partial x_j}\right] + C_{1\varepsilon}\frac{\varepsilon}{k}(G_k + C_{3\varepsilon}G_b) - C_{2\varepsilon}\rho\frac{\varepsilon^2}{k} + S_\varepsilon \tag{8}$$

where: G_k is the increase in the kinetic energy of turbulence caused by the gradient of average velocities, G_b stands for the energy generated by the phenomenon of buoyancy, Y_m is the energy associated with the fluid compressibility. $C_{1\varepsilon}$, $C_{2\varepsilon}$, and $C_{3\varepsilon}$ are constants of the model, whereas S_k, S_ε are, respectively, the turbulent Prandtl numbers. The turbulence specificity is determined using the parameters given by Equations (9)–(11), which are: intensity I, length scale l, and turbulent velocity μ_t.

$$I = 0.16 \cdot Re^{-0.125} \tag{9}$$

$$l = 0.07 \cdot D_H \tag{10}$$

$$\mu_t = \rho \cdot C_\mu \cdot k^2 \cdot \varepsilon^{-1} \tag{11}$$

where: Re is the Reynolds number and D_H is the relevant hydraulic diameter. The model constants were accepted using default values: $C_{1\varepsilon} = 1.44$, $C_{2\varepsilon} = 1.92$, $C_\mu = 0.09$, $\sigma_k = 1.0$, and $\sigma_\varepsilon = 1.3$. These values have been determined from experimental studies for fundamental turbulent flows [27] and are recommended by ANSYS [28].

3.5. Analysis Assumptions

The following assumptions were accepted for CFD analysis:

- The air velocity was constant at the inlet with the value $v_{inlet} = 10$ m/s.
- Air density $\rho = 1.225$ kg/m^3.
- Air viscosity $\mu = 1.7894 \times 10^{-5}$ kg/ms.
- Reynolds number $Re = 1.67 \times 10^3$

4. Results and Discussion

At first, the wind force acting on the longitudinal finned tubes in the wind direction was determined using CFD analysis and experimentally for each of the analyzed cases. The aerodynamic drag coefficients of the examined profiles were then calculated according to Equation (3) and summarized in Table 1.

Table 1. Results of experimental and CFD analyses.

Case	Velocity [m/s]	A_{ref_exp} [m^2]	A_{ref_CFD} [m^2]	F_{w_exp} [N]	F_{w_CFD} [N]	$cf_{\_exp}$ [–]	$cf_{\_CFD}$ [–]	($cf_{\_CFD}$-$cf_{\_exp}$) [–]	$cf_{\_error}$ [%]
c1	11.74	0.004	0.010	0.241	0.035	0.65	0.16	–	–
c2	9.67	0.013	0.009	1.009	0.856	1.40	1.49	0.10	7%
c3	9.63	0.013	0.010	1.000	0.824	1.39	1.45	0.06	4%
c4	10.54	0.010	0.007	0.813	0.674	1.23	1.37	0.14	10%
c5	10.05	0.013	0.003	0.764	0.642	0.98	1.04	0.06	6%
c6	10.03	0.012	0.010	0.762	0.656	1.05	1.14	0.10	8%

Where: exp, CFD—experimental, CFD calculations; A_{ref_exp}, A_{ref_CFD}—the reference area calculated as the area of the perpendicular projection of the analyzed tube in the air flow direction; F_{w_exp}—wind force obtained from experimental measurements by means of the force balance; F_{w_CFD}—wind force obtained from CFD analysis; $cf_{\_exp}$, $cf_{\_CFD}$—aerodynamic drag coefficient calculated in accordance with Equation (3); $cf_{\_error}$—percentage relative error.

The other results of CFD analysis are shown in Figures 9–14 as pressure distributions and velocity magnitude distributions. The results are presented in a plane parallel to the zx plane and located at the middle of the finned tube height. Comparing the local maximum pressure values that occurred on the finned tube profiles on the wind action side, it can be noticed that the highest value was obtained for the case c2 (profile with two fins), where the pressure was 133 Pa, followed by case c3 (profile with four fins), where the pressure was 124 Pa. This value was about 7% lower than the reported maximum. In the other cases, the

local maximum pressure values on the fins were 12–15% lower than the reported maximum pressure. On the other hand, comparing the velocity magnitude distributions, it can be noted that for the cases c2 and c3 there was the greatest increase in velocity at the edges of the profiles. In turn, for cases c4–c6, the peak velocity values were similar and the velocity distributions were very similar for those three cases.
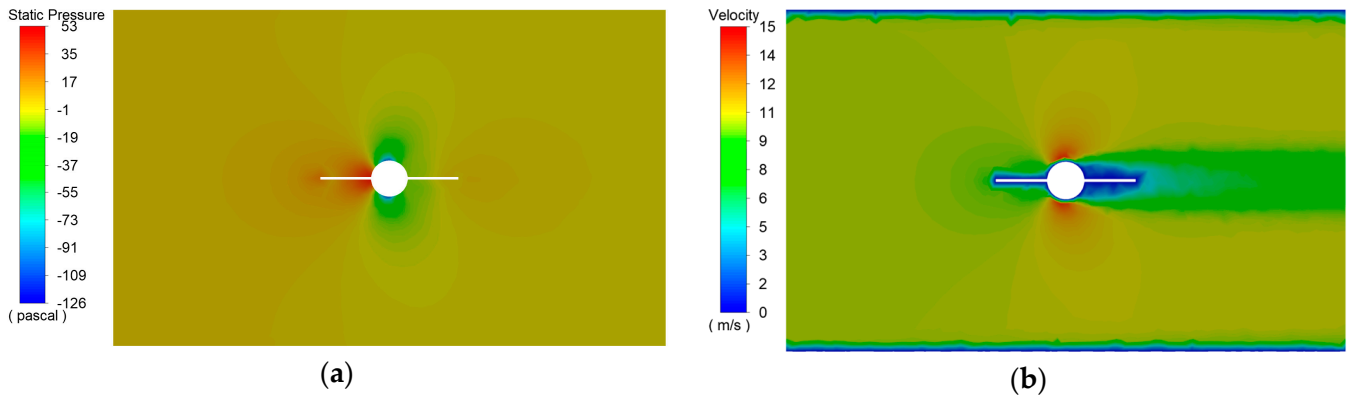

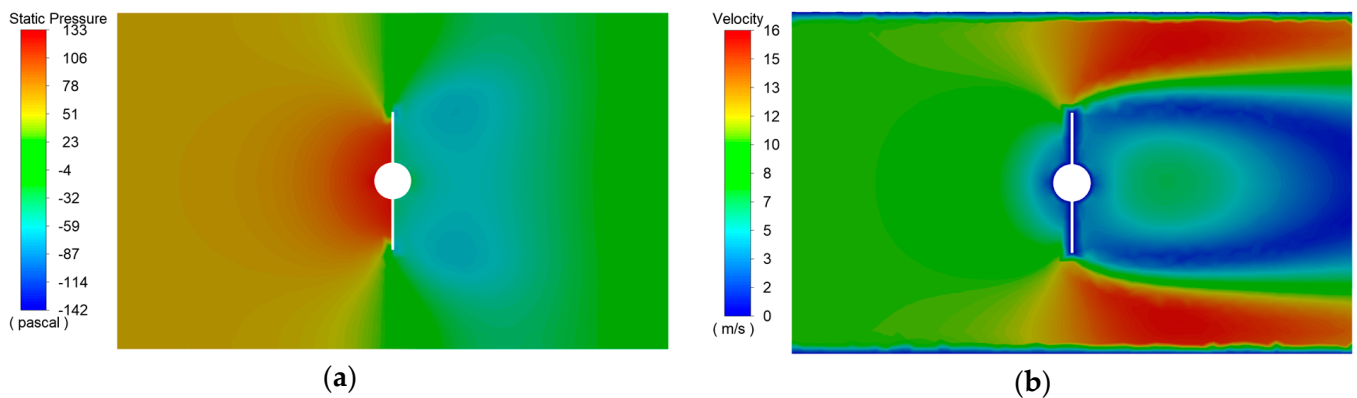**Figure 9.** (**a**) Pressure distribution; (**b**) Velocity distribution for the tube with 2 fins (case c1).

Figure 10. (**a**) Pressure distribution; (**b**) Velocity distribution for the tube with 2 fins (case c2).
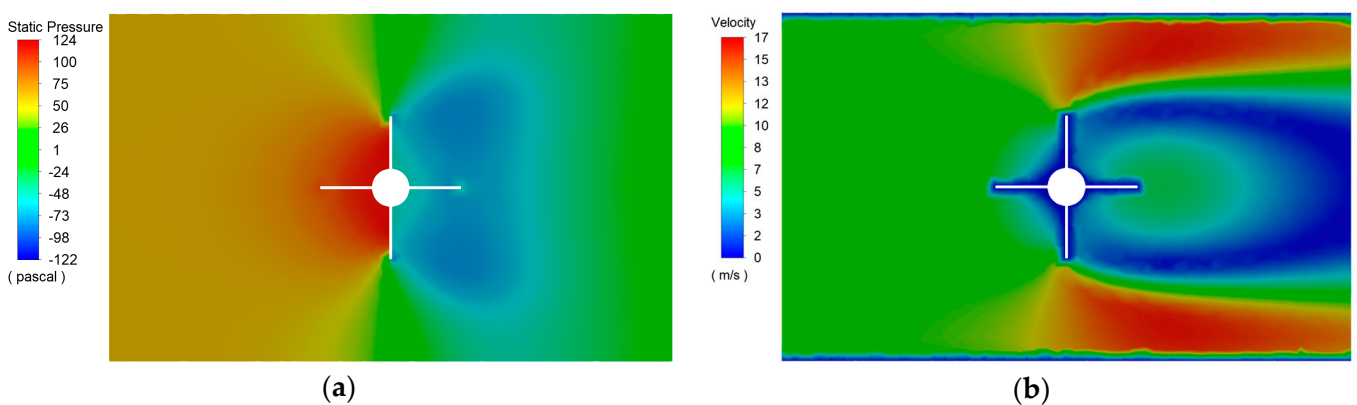

Figure 11. (**a**) Pressure distribution; (**b**) Velocity distribution for the tube with 4 fins (case c3).
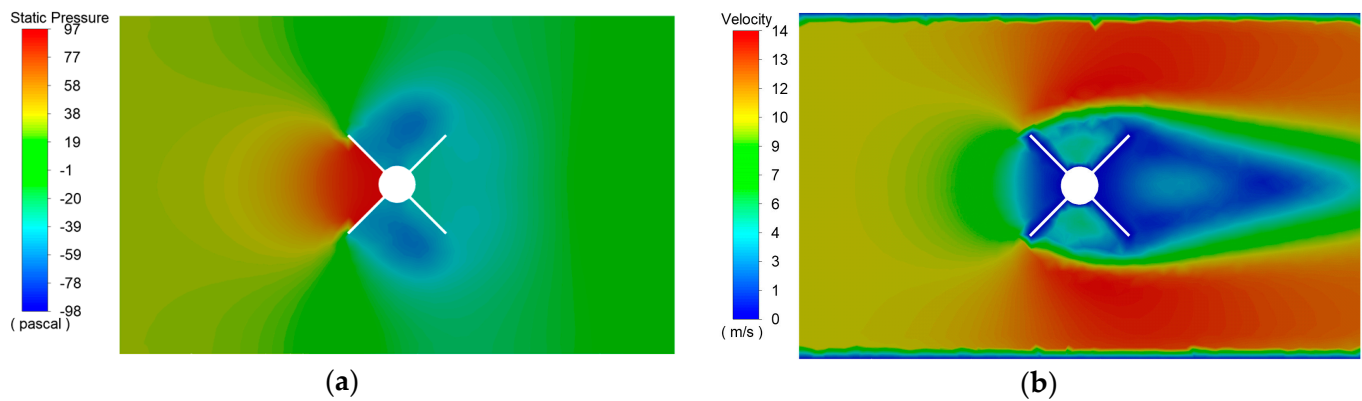
Figure 12. (**a**) Pressure distribution; (**b**) Velocity distribution for the tube with 4 fins (case c4).
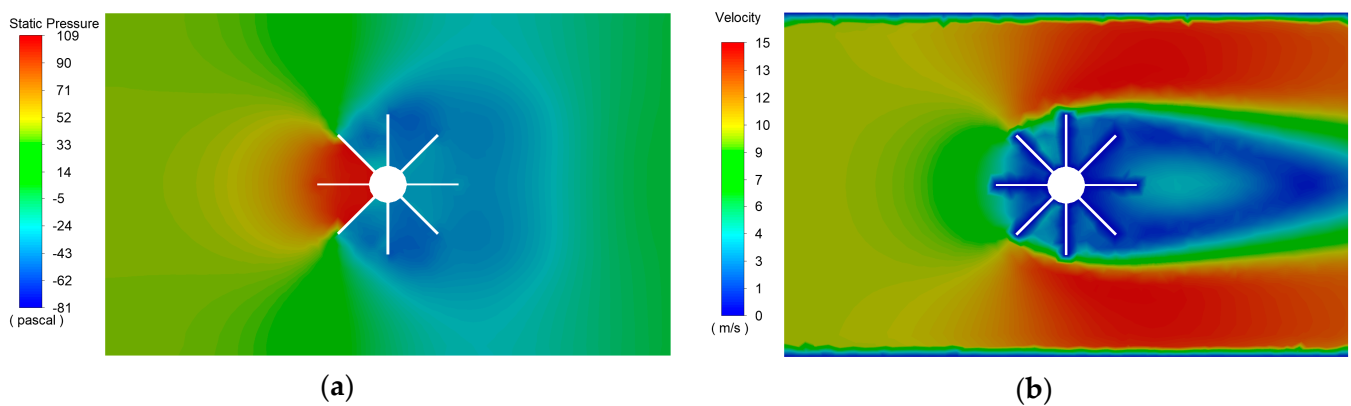

Figure 13. (**a**) Pressure distribution; (**b**) Velocity distribution for the tube with 8 fins (case c5).
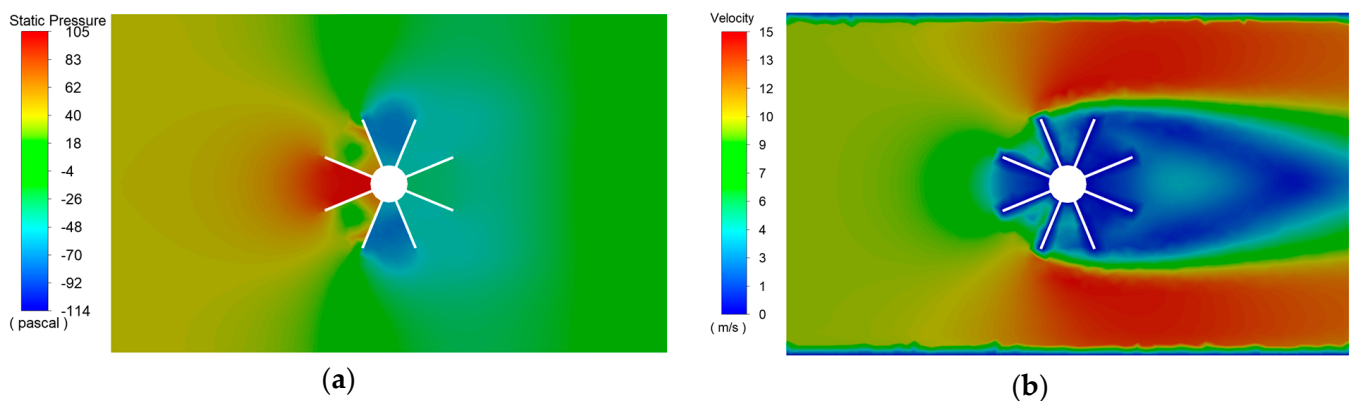

Figure 14. (**a**) Pressure distribution; (**b**) Velocity distribution for the tube with 8 fins (case c6).

For each of the analyzed cases, except for the case c1, the aerodynamic drag coefficients obtained by the CFD method were, respectively, higher than the values obtained from the experiment. The differences ranged from 0.06 to 0.14, which is from 4% to 10%. These differences result from the fact that in the case of the experimental tests, the finned tube profiles were mounted on a cylindrical support of the force balance. Additionally, a short length of cylindrical pipe protruded at the top of the finned tube profiles. The reference areas of those elements were included in the calculations. In turn, in the CFD analysis, the cylindrical support of the force balance and the short tube section at the top were not modeled, which is reflected in the results.

Consistently considering the case c1, one notices a significant difference in the CFD and experimental results. This result was also affected by the cylindrical support of the force balance. The arrangement of the two fins along the direction of the airflow separated the stream and resulted in a low value of the drag coefficient of 0.016 for CFD analysis. In contrast, the experimental result was 0.65, which was practically a coefficient typical for a cylindrical shape [29], or more specifically for a cylindrical support of the force balance.

However, despite some slight discrepancies between the numerical and experimental results, it can be seen that for cases c2–c6, both the CFD and the experimental results showed an analogous trend, which made it possible to compare the results for these cases. The highest values of the aerodynamic drag coefficients that were obtained for case c2 referred to the profile with two fins. The second highest result was obtained for the case c3, which concerned the profile with four fins. In both cases finned tube profiles were oriented so that the two fins in the profile section were a surface perpendicular to the direction of the airflow. The smallest value of the drag coefficient was obtained for case c5, which concerned a profile with eight fins rotated by 22.5° to the direction of airflow. On the other hand, for cases c5 and c6, which concerned profiles with eight fins, it was noted that the aerodynamic drag coefficients were very similar and it can be concluded that with a higher number of fins, the orientation of the profile did not have a major impact on the value of the aerodynamic drag coefficient.

5. Conclusions

When designing the LNG ambient air vaporizers, it is necessary to determine the maximum loads acting on the longitudinally finned tubes and verify whether the strength conditions are met. The design of ambient air vaporizers consists of aluminum longitudinal finned tubes that are subjected to internal pressure, thermal, seismic, and wind loads. The combined effect of all the above loads must be examined in the design calculations.

CFD analysis can be used to determine the wind load, or calculations can be performed according to the relevant standards for the wind load of the structure. However, this requires assuming values for the corresponding aerodynamic drag coefficients of longitudinal finned tubes.

In this study, aerodynamic drag coefficients were determined for longitudinal finned tubes with different numbers of fins. The various wind directions were also investigated.

The aerodynamic drag coefficients for the analyzed profiles were determined based on the results obtained from CFD analysis. Numerical results were compared with experimental results obtained on the wind tunnel test stand. The determined aerodynamic drag coefficients for different cross sections of finned tube profiles can be used to calculate the wind force acting on individual profiles.

References

1. Lisowski, E.; Czyżycki, W. Transport and storage of LNG in container tanks. *J. KONES Powertrain Transp.* **2011**, *18*, 193–201.
2. Lisowski, E.; Czyżycki, W.; Łazarczyk, K. Using of polyamide in construction of supporting blocks of cryogenic tanks on example of LNG container. *Arch. Foundry Eng.* **2010**, *10*, 81–86.

3. Lee, Y.; Na, J.; Lee, W.B. Robust design of ambient-air vaporizer based on time-series clustering. *Comput. Chem. Eng.* **2018**, *118*, 236–247. [CrossRef]
4. Lisowski, F.; Lisowski, E. Influence of Fins Number and Frosting on Heat Transfer through Longitudinal Finned Tubes of LNG Ambient Air Vaporizers. *Energies* **2022**, *15*, 280. [CrossRef]
5. Jeong, H.M.; Chung, H.S.; Lee, S.C.; Kong, T.W.; Yi, C.S. Optimum design of vaporizer fin with liquefied natural gas by numerical analysis. *J. Mech. Sci. Technol.* **2006**, *20*, 545–553. [CrossRef]
6. Niezgoda-Żelasko, B.; Żelasko, J. Free and forced convection on the outer surface of vertical longitudinally finned tubes. *Exp. Therm. Fluid Sci.* **2014**, *57*, 145–156. [CrossRef]
7. Kopeć, P.; Niezgoda-Żelasko, B. Optimisation of the Geometric Parameters of Longitudinally Finned Air Cooler Tubes Operating in Mixed Convection Conditions. *Processes* **2021**, *9*, 111. [CrossRef]
8. Sun, B.; Wadnerkar, D.; Utikar, R.P.; Tade, M.; Kavanagh, N.; Faka, S.; Evans, G.M.; Pareek, V.K. Modeling of Cryogenic Liquefied Natural Gas Ambient Air. *Ind. Eng. Chem. Res.* **2018**, *57*, 9281–9291. [CrossRef]
9. Wang, J.; Li, C.; Jia, W.; Wang, K. Study on the Heat Transfer Characteristics of an Ambient Air Vaporizer with Multi-Component Fluids. *Processes* **2022**, *10*, 851. [CrossRef]
10. Jeong, H.M.; Lee, Y.H.; Ji, M.K.; Bae, K.Y.; Chung, H.S. Natural convection heat transfer estimation from a longitudinally finned vertical pipe using CFD. *J. Mech. Sci. Technol.* **2009**, *23*, 1517–1527. [CrossRef]
11. Chen, S.; Yao, S.; Xie, F. Analysis of thermal conductivity of frost on cryogenic finned-tube vaporizer using fractal method. *Energy Power Eng.* **2013**, *5*, 109–115. [CrossRef]
12. Kuang, Y.; Yi, C.; Wang, W. Numerical simulation of frosting behavior and its effect on a direct-contact ambient air vaporizer. *J. Nat. Gas Sci. Eng.* **2015**, *27*, 55–63. [CrossRef]
13. Liu, S.; Jiao, W.; Wang, H. Three-dimensional numerical analysis of the coupled heat transfer performance of LNG ambient air vaporizer. *Renew. Energy* **2016**, *87*, 1105–1112. [CrossRef]
14. Liu, S.; Jiao, W.; Ren, L.; Wang, H.; Zhang, P. Dynamic heat transfer analysis of liquefied natural gas ambient air vaporizer under frost conditions. *Appl. Therm. Eng.* **2017**, *110*, 999–1006. [CrossRef]
15. Lee, Y.; Park, J.; Han, C. Modeling and Analysis of Frost Growth in Pilot-Scale Ambient Air Vaporizer. *Ind. Eng. Chem. Res.* **2018**, *57*, 5933–5943. [CrossRef]
16. Liu, S.; Jiao, W.; Ren, L.; Tian, X. Thermal resistance analysis of cryogenic frosting and its effect on performance of LNG ambient air vaporizer. *Renew. Energy* **2020**, *149*, 917–927. [CrossRef]
17. Lisowski, F.; Lisowski, E. Influence of Longitudinal Fin Tubes Arrangement in LNG Ambient Air Vaporizers on the Wind Load. *Energies* **2022**, *15*, 405. [CrossRef]
18. CEN. *Eurocode 1: Actions on Structures—Part 1–4: General Actions—Wind Actions*; EN 1991-1-4; European Committee for Standardization: Brussels, Belgium, 2005.
19. Matys, P.; Augustyn, M. Experimental determination of aerodynamic coefficients of different types of merry-go-round rotor blades. *Tech. Trans.* **2011**, *3*, 95–102.
20. Wu, G.; Zhang, L.; Yang, K. Development and Validation of Aerodynamic Measurement on a Horizontal Axis Wind Turbine in the Field. *Appl. Sci.* **2019**, *9*, 482. [CrossRef]
21. Zaghi, S.; Muscari, R.; Mascio, A.D. Assessment of blockage effects in wind tunnel testing of wind turbines. *J. Wind. Eng. Ind. Aerodyn.* **2016**, *154*, 1–9. [CrossRef]
22. Augustyn, M. Wind Action on a Mobile Elevating Work Platform (MEWP) in Operational Conditions. *Adv. Mater. Res.* **2014**, *1030–1032*, 1375–1378. [CrossRef]
23. Damjanović, D.; Kozak, D.; Holik, M. Analysis of wind influence to static stability of the eave framework. *Teh. Vjesn.* **2017**, *24*, 105–109. [CrossRef]
24. Flaga, A.; Kłaput, R.; Augustyn, M. Wind tunnel tests of two free-standing lighting protection masts in different arrangements with surroundings roof objects and roof conditions. *Eng. Struct.* **2016**, *124*, 539–548. [CrossRef]
25. Skeide, A.K.; Bardal, L.M.; Oggiano, L.; Hearst, R.J. The significant impact of ribs and small-scale roughness on cylinder drag crisis. *J. Wind. Eng. Ind. Aerodyn.* **2020**, *202*, 104192. [CrossRef]
26. ANSYS. *Intro to Governing Equations of Fluid Dynamics*; ANSYS Inc.: Canonsburg, PA, USA, 2020; Available online: http://www.ansys.com (accessed on 19 October 2022).
27. Launder, B.E.; Spalding, D.B. *Lectures in Mathematical Models of Turbulence*; Academic Press: London, UK, 1972.
28. *ANSYS Fluent Theory Guide, Release 2021 R2*; ANSYS Inc.: Canonsburg, PA, USA, 2021.
29. Blevins, R.D. *Applied Fluid Dynamics Handbook*; Krieger Publishing Company: Malabar, FL, USA, 2003.